Zhang *et al. J Wireless Com Network* (2022) 2022:41
https://doi.org/10.1186/s13638-022-02120-8

EURASIP Journal on Wireless Communications and Networking

RESEARCH Open Access

A practical underwater information sensing system based on intermittent chaos under the background of Lévy noise

Hanwen Zhang[1], Zhen Qin[3], Yichao Zhang[2], Dajiang Chen[3], Ji Gen[3*] and Hao Qin[1]

*Correspondence: jgeng@uestc.edu.cn
[3] Network and Data Security Key Laboratory of Sichuan Province, Chengdu, China
Full list of author information is available at the end of the article

Abstract

Nowadays, the increasingly complex and changeable marine environment makes the signals received by the underwater sensing equipment not only contain the weak signals radiated by underwater targets but also accompanied by marine solid background noise, which leads to the degradation and distortion of underwater acoustic signals and the decline of underwater communication quality. Under the severe influence of ocean noise, the underwater acoustic sensing and acquisition system will have the problems of high SNR ratio threshold, minimal sensing bandwidth, and unable to sense the signal with unknown frequency effectively. The Lévy noise model has been selected to describe the marine noise environment and explain its scientificity in this paper. A parameter estimation method for Lévy noise is proposed. Under the condition of characteristic index $\alpha = 1.5$ and noise intensity $D = 0.1$of the Lévy noise model, the estimated mean values of parameters are 1.5026 and 1.1664. The estimated variances are 0.0034 and 0.0046, which proves the effectiveness and applicability of the estimation method. Then, an improved dual-coupled Duffing oscillator sensing system is proposed to sense the weak signals with unknown frequency under Lévy noise. Under the background of Lévy with characteristic index $\alpha = 1.5$, deflection parameter $\beta = 0$ and noise intensity $D = 0.1$, the sensing error rate of our system with unknown frequency is 0.054%, the lowest sensing signal amplitude is $A = 0.010$, the lowest sensing SNR ratio is -23.9254 dB, and the frequency of multi-frequency weak signals to be measured can be obtained. The estimation error of frequency sensing is 0.33%.

Keywords: Underwater information sensing, Lévy noise, Chaotic oscillator

1 Introduction

With the progress of modern technology, e.g., Internet of things (IoT) [1–3], data communication [4], artificial intelligence (AI) [5–8] and cloud computing [9, 10], the research on marine exploration and other related fields is gradually increasing, the stealth of underwater targets seems to be improving, and the radiated energy is getting lower and lower. This makes the weak underwater signal sensing in the marine environment a complex problem perplexing the development of underwater acoustics, especially for the weak signal of unknown frequency [11, 12]. At the same time, due to the variability of the marine environment, the signal received by the underwater sensing equipment not

only contains the weak signal radiated by the target but is also accompanied by the solid marine background noise, which leads to the degradation and distortion of the acoustic signal and the decline of the communication quality [13, 14]. Through the derivation of the central limit theorem, underwater acoustic noise can be briefly described as Gaussian noise [15], so most of the current studies choose the Gaussian noise model for discussion. However, in the actual marine environment, few active will dominate in a specific frequency range, and there is random non-Gaussian impulse noise in the signal, which has more severe tailing than Gaussian noise. When using Gaussian noise to simulate and design the algorithm, it will have a significant impact on the performance of the sensing system [16–19]. Therefore, it is necessary to study the underwater acoustic noise model and underwater weak signal sensing method.

In the study of marine noise, the noise interference of the underwater environment often contains intense pulses, which do not conform to Gaussian distribution [20–22]. Non-Gaussian noise does not have Markov characteristics, which is very difficult to deal with in the research of weak signal sensing [23]. Albeverio, Kondratiev and others extended HIDA's theory to the case of non-Gaussian [24–26]. Fan and others used the statistical characteristics of high-order accumulation to analyze ocean noise [27] in 2018, but this method cannot fully describe the characteristics of non-Gaussian. Later, after analysis by Lu, Nikias, Li and others, it was found that in addition to Cauchy, Lévy and Gaussian processes, the probability distribution has an unstable closed form [28]. Recently, Lévy noise has been one of the research hotspots of non-Gaussian noise analysis. Just as Gaussian noise can be regarded as the generalized time derivative of Brownian motion, Lévy noise can also be regarded as the generalized time derivative of the Lévy process, and it is a basic stationary independent incremental random process. Lévy distribution is a generalized form of Gaussian distribution. It is a typical non-Gaussian noise with a long tail, discontinuous jump and infinite separability. It can maintain the natural noise process's generation mechanism and propagation conditions. The Lévy noise model established by Lévy distribution can describe many symmetrical or asymmetric noises with different impulsivity by controlling the selection of different parameters [29, 30]. It has more substantial applicability and great significance to describe the influence characteristics of underwater environmental noise interference [31]. Therefore, selecting the Lévy model parameters in different application scenarios is also one of the research objects of this paper.

In terms of weak underwater signal sensing methods, some classical signal processing methods become difficult to apply due to the increasingly low signal-to-noise ratio of signals received by underwater equipment. For example, wavelet transform will have the problem that the basis function cannot be effectively selected [32]. Although stochastic resonance can realize the sensing of weak signals, it cannot accurately perceive signals with large amplitude and frequency, and there is the problem of how to select parameters [33] effectively. At present, scholars worldwide have shown great interest in chaos theory. In the 1990s, chaos theory began to be used for signal sensing. In order to solve the problems of high signal-to-noise ratio threshold and limited sensing bandwidth, coupled Duffing oscillator algorithm [34] appeared, coupling Duffing oscillator and Van der Pol Duffing oscillator algorithm [35], bidirectional ring coupling Duffing oscillator transient synchronization breakthrough method [36], etc. These algorithms improve the solution speed to a certain

extent, but there is still a problem that the unknown frequency signal with a low signal-to-noise ratio is complex to perceive [37–44].

This paper proposes an underwater position sensing method that is more suitable for weak signals in a complex ocean environment to solve the above problems. The main contributions of this paper are as follows:

- Lévy noise model is proposed to describe the underwater natural environment, and an analysis and estimation method is provided to select better parameters.
- Aiming at the sensing problem of weak underwater signal with unknown frequency, and improved dual-coupled Duffing oscillator signal sensing method based on scale change and variable step size is proposed. This method has better resistance to intense noise, better adaptability to impact noise, higher sensing efficiency, more intuitive sensing results, and a lower threshold.
- An underwater weak signal sensing system with unknown frequency is designed and established. The system can better sense multi-frequency signals under the Lévy noise model. The feasibility and superiority of the sensing system established in this paper are verified by using the actual underwater acoustic data.

2 Related work

2.1 Lévy noise model

The Lévy process was proposed by the French mathematician Paul Lévy to study the generalized central limit theorem. It is a random process with independent and fixed increments, indicating that the movement of a point and its continuous displacement are random [45]. The difference between two disjoint time intervals displacement is independent. The displacement and displacement in different time intervals of the same length have the same probability distribution. It can be regarded as a continuous-time simulation of random walk. Lévy noise also called alpha noise obeys the theory of stable alpha distribution. The only distribution satisfies the generalized central limit theorem, and a square law attenuates its tailing. The expression of the characteristic function of Lévy noise [46] is as follows:

$$log\varphi(t) = \begin{cases} -\sigma^{\alpha}|t|\left\{1 - i\beta sign(t)tan\left(\frac{\pi\alpha}{2}\right)\right\} + i\mu t, \ \alpha \neq 1 \\ -\sigma|t|\left\{1 + i\beta sign(t)\frac{\pi}{2}log(|t|)\right\} + i\mu t, \ \alpha = 1 \end{cases} \tag{1}$$

$$\begin{cases} X &= S_{\alpha,\beta}\frac{sin(\alpha(V+B_{\alpha,\beta}))}{(cosV)^{\frac{1}{\alpha}}}\left(\frac{cos(V-\alpha(V+B_{\alpha,\beta}))}{W}\right)^{\frac{1-\alpha}{\alpha}}, \ \alpha \neq 1 \\ X &= \frac{2}{\pi}\left[\left(\frac{\pi}{2} + \beta V\right)tanV - \beta log\left(\frac{WcosV}{\frac{\pi}{2}+\beta V}\right)\right], \qquad \alpha = 1 \end{cases} \tag{2}$$

In (1), $\alpha \in (0, 2]$ is the characteristic index, which determines the decay rate of the distribution tail. When $\alpha = 1$, it is Cauchy distribution. When $\alpha = 2$, it is the Gaussian distribution, and the mean value is μ, the variance is $2\sigma^2$. When $\alpha \neq 2$, the mean value is μ, but the variance does not exist. $\beta \in [-1, 1]$ is the skew parameter. When $\beta = 0$, the graph is symmetrical, and when β is a positive number, The graph tilts to the right; on the contrary, the graph tilts to the left, $\sigma > 0$ is the scale parameter, which determines the degree of dispersion of the distribution concerning μ and $\mu \in R$ is the position

parameter. The left and right translation can be achieved by adjusting the value of μ. Rfal-Weron proved the expression of Lévy distribution random variable. In (2), V obeys the uniform distribution in the interval $(-2\pi, 2\pi)$, W follows the exponential distribution with the mean value 1, $S_{\alpha\beta}$ and $B_{\alpha\beta}$ is as follows:

$$S_{\alpha,\beta} = \left[1 + \beta^2 tan^2 \frac{\pi\alpha}{2}\right]^{1/2\pi} \tag{3}$$

$$B_{\alpha,\beta} = \frac{arctan\left(\beta tan\frac{\pi\alpha}{2}\right)}{2} \tag{4}$$

Under the conditions of $\beta = 0$, $\sigma = 1$ and $\mu = 0$, the Lévy distributions corresponding to different α feature indices are shown in Fig. 1.

It can be seen from Fig. 1 that the smaller the value α, the stronger the impact of noise interference. When $\alpha = 2$, the noise interference has almost no impact. At this time, the Lévy noise degenerates into white noise.

2.2 Intermittent chaotic oscillator sensing system

2.2.1 Intermittent chaos of single Duffing oscillator

At present, in sensing weak signals with unknown frequency, the commonly used method is to use the intermittent chaotic characteristics of the chaotic system. Using the phase change of chaotic oscillator to sense weak periodic signal requires a slight frequency difference between the signal to be measured and the decision power in the

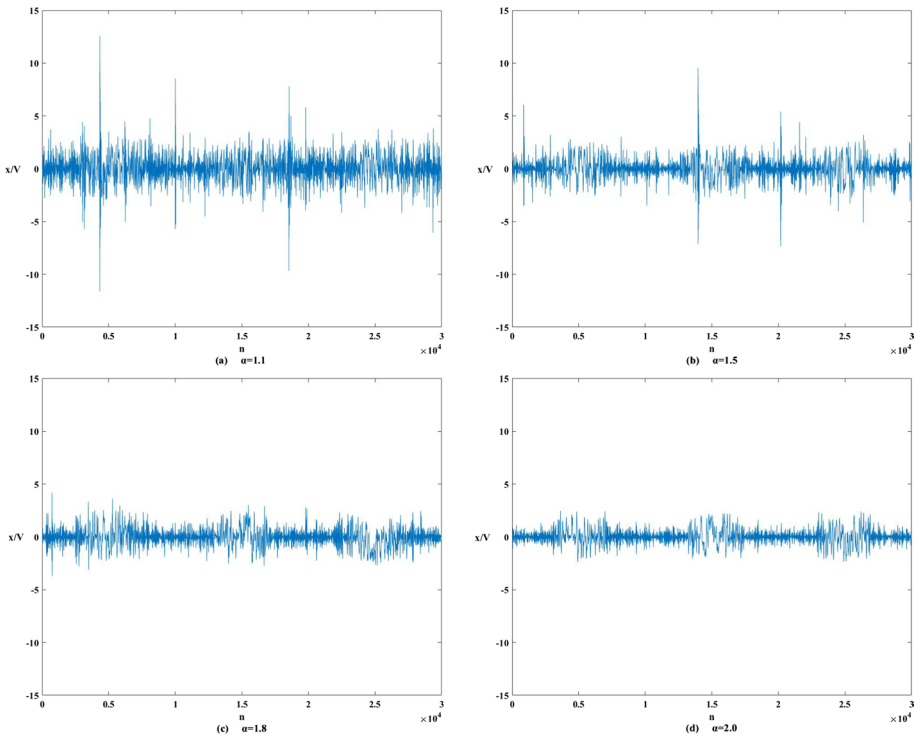

Fig. 1 Time-domain distribution map of live noise corresponding to different feature index α

established chaotic sensing system. This frequency difference will lead to chaos and periodic intermittent chaos in the sensing system. Intermittent chaos uses the immunity of chaotic oscillator to noise and the sensitivity to weak signal disturbance to sense periodic noise signals with unknown frequency.

Make the signal input into the single Duffing oscillator chaos sensing system as $f(t)$, $f(t) = Acos[(\omega + \Delta\omega t) + \varphi]$, $\Delta\omega$ is the frequency difference between the signal input into the chaotic sensing system and the periodic force between the chaotic system, $\Delta\omega \ll \omega$, φ is the phase difference. At this time, the state equation of single Duffing oscillator system can be expressed as [41, 47, 48]:

$$\begin{cases} \dot{x} &= \omega y \\ \dot{y} &= \omega\left[-\frac{1}{2}y + x - x^3 + \gamma cos(\omega t) + f(t)\right] \end{cases} \tag{5}$$

where γ is the critical chaotic threshold, and the total dynamic force of the single Duffing oscillator system is:

$$\begin{aligned} L(t) &= \gamma\cos(\omega t) + A\cos[(\omega + \Delta\omega t) + \varphi] + \eta(t) \\ &= \gamma\cos(\omega t) + A\cos(\omega t)\cos(\Delta\omega t + \varphi) - A\sin(\omega t)\sin(\Delta\omega t + \varphi) + \eta(t) \\ &= \mathrm{P}(t)\cos[\omega t + \theta(t)] + \eta(t) \end{aligned} \tag{6}$$

$$P(t) = \sqrt{\gamma^2 + 2A\gamma\cos(\Delta\omega t + \varphi) + A^2} \tag{7}$$

$$\theta(t) = \arctan\frac{A\sin(\Delta\omega t + \varphi)}{\gamma + A\cos(\Delta\omega t + \varphi)} \tag{8}$$

where $A \ll \gamma$, therefore, $\theta(t)$ is small enough, so its effect on the dynamics of the chaotic system can be ignored. This analysis shows that:

- If $\Delta\omega = 0$, the real influential parameter for the motion state of the system is the phase difference φ. When there is $\pi - \arccos(\frac{A}{2\gamma}) \le \varphi \le \pi + \arccos(\frac{A}{2\gamma})$ and $\mathrm{P}(t) \le \gamma$, the chaotic sensing system will still be in a chaotic state. If φ does not meet this condition, the system will quickly change to a large-scale periodic state.
- If $\Delta\omega \neq 0$, then $L(t)$ will deviate from γ with $\mathrm{T} = \frac{2\pi}{\Delta\omega}$ as the period. In this state, the system will enter a regular intermittent chaotic state, which is manifested as the state of chaotic sensing system. The chaotic state and large-scale periodic state appear in a stable, regular and periodic alternating manner. The sensing of weak signals with unknown frequency is based on this.
- If the value of $\Delta\omega$ is too large, the system policy power of the chaotic sensing system will change too fast so that the system cannot respond quickly. When there is a large difference between the frequency of the weak signal to be measured and the system policy power, even if the signal amplitude input to the sensing system is large enough, the system will not have phase transition and regular, stable and periodic intermittent chaotic motion.

From the above analysis and discussion, it is found that the method of using the intermittent chaos theory of chaotic oscillator to sense the weak periodic signal of

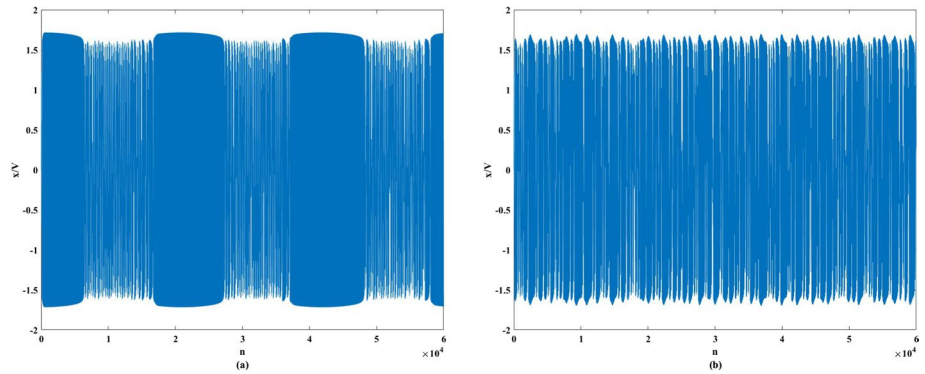

Fig. 2 The output sequence of the single Duffing oscillator system

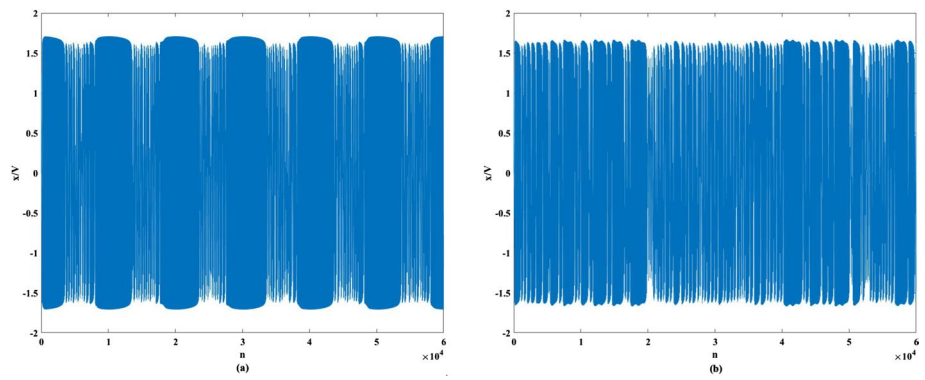

Fig. 3 The output sequence of the dual-coupled Duffing oscillator system

position frequency is scientific and effective. Through the simulation, it is found that in the single Duffing oscillator chaotic sensing system, when $\left|\frac{\Delta\omega}{\omega}\right| \leq 0.03$, the output sequence of the system is shown in Fig. 2a, and it is observed that Fig. 2a is an obvious intermittent chaotic state. When $\left|\frac{\Delta\omega}{\omega}\right| > 0.03$, the timing diagram of system output cannot be judged as intermittent chaotic state, as shown in Fig. 2b.

2.2.2 Intermittent chaos of double coupled Duffing oscillator

Make the signal to be measured to be input into the dual-coupled Duffing oscillator chaos sensing system as $f(t)$, $f(t) = Acos[(\omega + \Delta\omega t) + \varphi]$, $\Delta\omega$ is the frequency difference between the signal to be measured input into the chaotic sensing system and the periodic force between the chaotic system, $\Delta\omega \ll \omega$, φ is the phase difference. At this time, the state equation of dual-coupled Duffing oscillator system can be expressed as:

$$\begin{cases} \ddot{x}(t) + k\dot{x}(t) - x(t) + x^3(t) + d[y(t) - x(t)] = \gamma\cos(\omega t) + f(t) \\ \ddot{y}(t) + k\dot{y}(t) - y(t) + y^3(t) + d[x(t) - y(t)] = \gamma \mathrm{F}\cos(\omega t) + f(t) \end{cases} \tag{9}$$

where $f(t) = Acos(\dot{\omega}t + \varphi)$, $\dot{\omega} = \omega + \Delta\omega$. When $\left|\frac{\Delta\omega}{\omega}\right| \leq 0.08$, the output sequence of the system is shown in Fig. 3a, which is an obvious intermittent chaotic state. When

$\left|\frac{\Delta\omega}{\omega}\right| > 0.08$, the timing diagram of the system output cannot be judged as an intermittent chaotic state, as shown in Fig. 3b.

3 Methods

3.1 Parameter analysis and estimation of Lévy noise model

The Fokker-Plank equation corresponding to equation (10) is:

$$\frac{\partial_p(s,t)}{\partial t} = \left[\frac{\partial}{\partial x}A(x) + \frac{\partial^2}{\partial x}B(x)\right]\rho(s,t) \tag{10}$$

where $A(x) = ax - bx^3 + S(x)$, $B(x) = D$. Since equation (11) is a transcendental equation, it cannot be solved directly, but the approximate number of equation (11) can be calculated using the finite difference method. The following equations can be obtained by using the fourth-order Runge--Kutta method.

$$\mathrm{v}_{i+1} = v_i + \frac{\Delta t}{6}(F_1 + 2F_2 + 2F_3 + F_4) + \Delta t^{\frac{1}{\alpha}}\eta_i \tag{11}$$

where Δt is the step size, $F_i(i = 1, 2, 3, 4)$ are:

$$\mathrm{F}_1 = -v_i^3 + (a+1)v_i^2 - \frac{a+b}{\gamma}v_i + v_i\sqrt{\frac{D}{\Delta t}}\xi_i \tag{12}$$

$$\begin{aligned}\mathrm{F}_2 = &-(v_i + \frac{\Delta t}{2}F_1)^3 + (a+1)(v_i + \frac{\Delta t}{2}F_1)^2 \\ &- \frac{a+b}{\gamma}(v_i + \frac{\Delta t}{2}F_1) + (v_i + \frac{\Delta t}{2}F_1)\sqrt{\frac{D}{\Delta t}}\xi_i\end{aligned} \tag{13}$$

$$\begin{aligned}F_3 = &-(v_i + \frac{\Delta t}{2}F_2)^3 + (a+1)(v_i + \frac{\Delta t}{2}F_2)^2 \\ &- \frac{a+b}{\gamma}(v_i + \frac{\Delta t}{2}F_2) + (v_i + \frac{\Delta t}{2}F_2)\sqrt{\frac{D}{\Delta t}}\xi_i\end{aligned} \tag{14}$$

$$\begin{aligned}F_4 = &-(v_i + \Delta t F_3)^3 + (a+1)(v_i + \Delta t F_3)^2 \\ &- \frac{a+b}{\gamma}(v_i + \Delta t F_3) + (v_i + \Delta t F_3)\sqrt{\frac{D}{\Delta t}}\xi_i\end{aligned} \tag{15}$$

The numerical solution of the Lévy noise model obtained according to the above method is shown in Fig. 4, where $\alpha = 1.5$, $\beta = 0$, $D = 0.1$.

Next, the influence of various parameters of Lévy noise model is further analyzed, including Lévy noise intensity D, stability index α and deflection parameter β.

Figure 5 shows the curve of probability density function $P_{st}(v)$ of Lévy noise model with different noise intensity, where $\alpha = 1.1$, $\beta = 0$. When the noise intensity $D = 0.1$, the image of $P_{st}(v)$ has two peaks, which indicates that there are two steady states in the process of particle motion, that is, the left peak and the right peak of the image. With the increase of noise intensity D, the image of $P_{st}(v)$ gradually changes from two peaks to a single peak structure with only one peak, which indicates that the noise intensity D

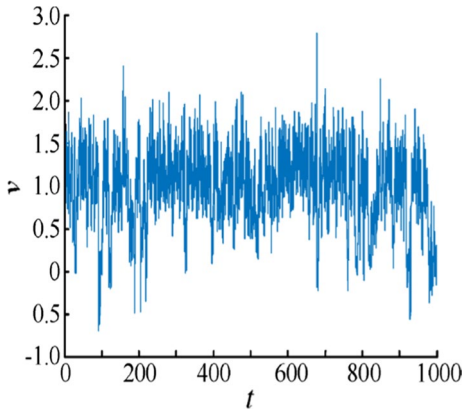

Fig. 4 The Lévy noise model

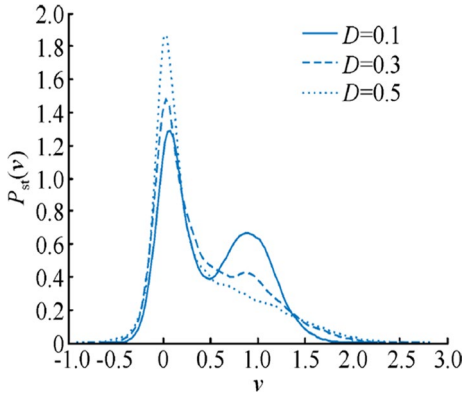

Fig. 5 The particle probability distribution of the system output under the excitation of different noise intensity D

in Lévy noise model can induce the phase transfer of particle system motion. When the noise intensity D is smaller, the movement of particles is more affected by the traction of the signal, and its density curve is relatively smooth. When the noise intensity D gradually increases to $D = 0.3$, the particles gradually concentrate on one side of the zero point. When the noise intensity D increases to $D = 0.5$, the particles are gradually unevenly distributed on both sides of the zero point. This phenomenon is analyzed from the microscopic point of view, that is, when the noise intensity $D < 0.3$, because the excitation intensity of the external noise is not enough, the energy obtained by the particles for motion is not enough make them cross the potential barrier. These particles can only move back and forth in a potential well, so the particles can only concentrate on one side of the zero point as for whether to move in the left potential well or the right potential well mainly depends on the combined force of the signal traction received by the particle at zero and the interference of external noise. When the noise intensity $D = 0.5$, the moving particles are strongly excited by the noise to obtain enough energy to jump over the potential barrier from one potential well to another. The noise will affect the change of particles, so the particles will not be symmetrically distributed on both sides of the zero point.

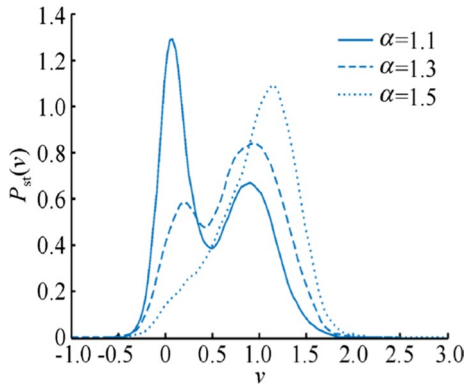

Fig. 6 The particle probability distribution of the system output under the excitation of different stability index α

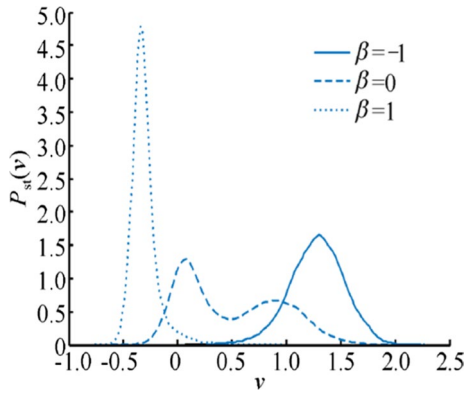

Fig. 7 The particle probability distribution of the system output under the excitation of different deflection parameter β

Figure 6 shows the curve of probability density function $P_{st}(v)$ of Lévy noise model with different stability index, where $D = 1, \beta = 0$. When $\alpha = 1.1$, the image of $P_{st}(V)$has two peaks. However, when the characteristic index αgradually increases, the left peak of $P_{st}(V)$image gradually decreases, and the right peak gradually increases. When $\alpha = 1$, the left peak of $P_{st}(v)$ disappears, and the image of $P_{st}(v)$ gradually changes from two peaks to a single peak structure with only one peak. This also shows that the characteristic index α in the Lévy noise model can induce particle system motion phase transfer. From the microscopic point of view, the barrier height is low when α is small. At this time, although the energy obtained by the particles is small, they can cross the barrier by their energy. With the gradual increase of characteristic index a, the height of the potential barrier is also increasing. Therefore, particles need to obtain certain energy from noise to cross the potential barrier. If the noise intensity D does not change, particles cannot cross the potential barrier.

Figure 7 shows the curve of probability density function $P_{st}(v)$ of Lévy noise model with different deflection parameters. When $\beta = -1$, the image of $P_{st}(v)$ has and only has one peak. The function has two peaks as the skew parameter β increases from -1 to 0. This indicates that the skew parameter β of the Lévy noise model can induce the phase transfer

of particle system motion. When the skew parameter β increases further, the right peak of $P_{st}(v)$ begins to decrease slowly. On the contrary, the left peak of $P_{st}(v)$ begins to rise slowly. When the skew parameter β increases to $\beta = 1$, the right peak of $P_{st}(v)$ disappears and the left peak continues to rise. The phenomenon is analyzed from a microscopic point of view. With the increase of the deflection parameter β, the potential barrier height that the particles need to cross is smaller. When the deflection parameter $\beta = -1$, the potential barrier height that the particles need to cross is very high. When the energy cannot be obtained through the external excitation noise, the particles cannot cross the potential barrier and can only move back and forth on one side. With the increase of the deflection parameter β, the barrier height decreases, and less energy is required for particles to enter from one potential well to the other. Through the above research and analysis, it can be found that the establishment of the Lévy noise model requires a good selection of three parameters: characteristic index α, deflection parameter β, and Lévy noise intensity D. In general, it is considered that the underwater environmental noise is unbiased, and the position parameter is 0. Therefore, when constructing the underwater Lévy noise model, we only need to pay attention to the characteristic index α and Lévy noise intensity D of Lévy noise to generate a more applicable Lévy noise model to describe underwater noise.

In this regard, this paper quotes the method of literature [49], to estimate the characteristic index α and the noise intensity D of the Lévy noise model:

$$E\left(|X|^{\rho}\right) = \frac{\rho lg\alpha}{\alpha lgD} C(\rho,\alpha) \tag{16}$$

where $E(|X|^{\rho})$ is the fractional low-order moment, and ρ is the order, $C(\rho,\alpha) = \frac{2^{\rho+1}\tau\left(\frac{\rho+1}{2}\right)\tau\left(\frac{-\rho}{\alpha}\right)}{\alpha\sqrt{\pi}\tau\left(\frac{-\rho}{2}\right)}$, $-1 < \rho < \alpha \leq 2$. Let $Y = lg|X|E(Y) < +\infty$, the moment generating function is:

$$E\left(|X|^{\rho}\right) = \lim_{\rho\to 0} \frac{d^q}{d\rho^q} E\left(|X|^{\rho}\right), q \in N^* \tag{17}$$

Since Y is only related to α except for the first moment, the first two finite logarithmic moments are listed as:

$$\begin{cases} G_1 &= E(|X|^{\rho}) = \Phi_0\left(1-\frac{1}{\alpha}\right) + lg\left|\frac{lg\alpha}{lgDcosk}\right|^{\frac{1}{\alpha}} \\ G_2 &= E\left[\left(lg|X| - E(Y)\right)^2\right] = \Phi_1\left(\frac{1}{2}+\frac{1}{\alpha^2}\right) - \left(\frac{k}{\alpha}\right)^2 \\ \Phi_0 &= \frac{dlg\tau(t)}{dt} \\ \Phi_1 &= \frac{d^2lg\tau(t)}{dt^2} \end{cases} \tag{18}$$

Let $t = 1$, then $\Phi_0 = -0.5772$ and $\Phi_1 = 1.6449$ are obtained. The estimated value can be obtained from the above formula:

$$\begin{cases} \widehat{\alpha} &= \left(\frac{G_2}{\Phi_1} - \frac{1}{2}\right)^{-\frac{1}{2}} \\ \widehat{D} &= e^{(\Phi_0 - G_1)\widehat{\alpha} - 1} \frac{lg\widehat{\alpha}}{cosk} \\ \left|\widehat{k}\right| &= \left[\left(\frac{\widehat{\alpha}^2}{2} - 1\right)\Phi_1 - G_1\widehat{\alpha}^2\right]^{\frac{1}{2}} \end{cases} \tag{19}$$

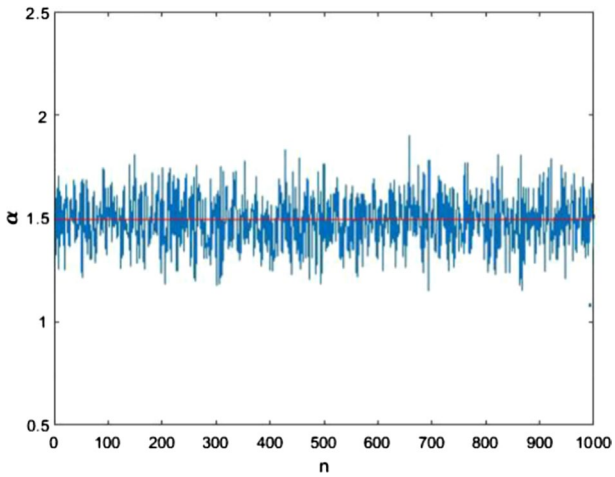

Fig. 8 Estimation of characteristic index α

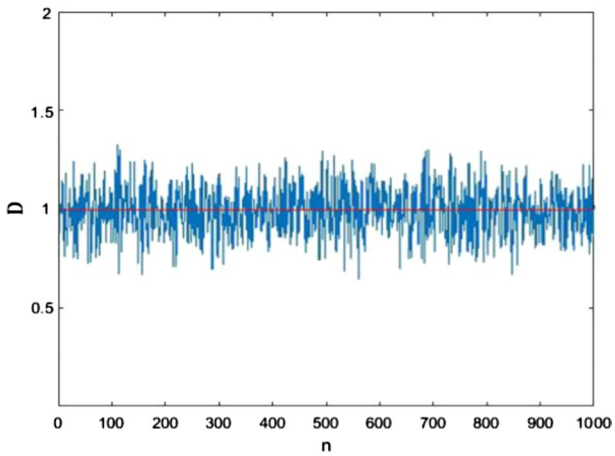

Fig. 9 Estimation of noise intensity D

To test the effectiveness of the estimation method, the Chambers-Mallows-Stuck (CMS) method is used to generate the Lévy noise with $\alpha = 1.5$, $D = 1$, and the parameters of α, D are estimated. The estimated results are shown in Figs. 8 and 9:

where n represents the number of estimates, Figs. 8 and 9 show that values of α and D are obtained, respectively, as 1.5026 and 1.1664; the estimated variance is 0.0034 and 0.0046, respectively. It proves that the method can estimate the parameters of interference noise in the actual underwater information sensing environment.

3.2 Improved signal sensing method based on the scale transformation of the variable step-size intermittent chaotic differential dual-coupled Duffing oscillator

3.2.1 Improved signal sensing method of intermittent chaotic dual-coupled Duffing oscillator

It is found that the combination of two oscillators in this paper has more robust stability than the coupling of two oscillators in theory so that the sensing of chaotic signals from the two oscillators can be better than that from the coupling of two oscillators in theory.

Moreover, the differential timing chart of the sensing system coupling two pairs of chaotic oscillators will make the sensing results more intuitive and easier to judge. When the sensing system is in a large-scale periodic state, the differential timing diagram will display a closed curve with relatively regular amplitude. When the sensing system is in a chaotic state, the differential timing diagram will show the irregular peak diagram with a large amplitude swing, which will be more conducive to observing the state of the chaotic sensing system. Therefore, the improved dual-coupled Duffing oscillator model is proposed in this paper:

$$\begin{cases} \ddot{x}_1 + c\dot{x}_1 - x_1 + x_1^3 + k(x_1 - x_2) = f\cos(\omega t) \\ \ddot{x}_2 + \mu(1 - x_2^3)\dot{x}_2 + x_2 + k(x_2 - x_1) = f\cos(\omega t) \\ \ddot{y}_1 + c\dot{y}_1 - y_1 + y_1^3 + k(y_1 - y_2) = \mathrm{F}f\cos(\omega t) \\ \ddot{y}_2 + \mu(1 - y_2^3)\dot{y}_2 + y_2 + k(y_2 - y_1) = \mathrm{F}f\cos(\omega t) \end{cases} \tag{20}$$

where F represents the dynamic coefficient of the periodic policy. The dual-coupled Duffing oscillator model contains two pairs of Duffing oscillators. The difference between the two pairs lies in the difference of the dynamic coefficient of the periodic policy, and other parameter conditions are exactly the same. Next, input the same signal to be tested into the system:

$$\begin{cases} \ddot{x}_1 + c\dot{x}_1 - x_1 + ax_1^3 + k(x_1 - x_2) = f\cos(\omega t) + A\cos(\omega_1 t) + \eta(t) \\ \ddot{x}_2 + \mu(1 - x_2^3)\dot{x}_2 + x_2 + k(x_2 - x_1) = f\cos(\omega t) + A\cos(\omega_1 t) + \eta(t) \\ \ddot{y}_1 + c\dot{y}_1 - y_1 + ay_1^3 + k(y_1 - y_2) = \mathrm{F}f\cos(\omega t) + A\cos(\omega_1 t) + \eta(t) \\ \ddot{y}_2 + \mu(1 - y_2^3)\dot{y}_2 + y_2 + k(y_2 - y_1) = \mathrm{F}f\cos(\omega t) + A\cos(\omega_1 t) + \eta(t) \end{cases} \tag{21}$$

where $f(t) = f\cos(\dot{\omega}t + \varphi)$, $\dot{\omega} = \omega + \Delta\omega$. Through the simulation, it is found that in the intermittent chaotic sensing system, when $\left|\frac{\Delta\omega}{\omega}\right| \leq 0.9$, the sequence diagram output by the intermittent chaotic sensing system is shown in Fig. 10, which can be judged as an obvious intermittent chaotic state, while when $\left|\frac{\Delta\omega}{\omega}\right| > 0.09$, the sequence diagram output by the intermittent chaotic sensing system is shown in Fig. 11, which cannot be judged as an intermittent chaotic state.

3.2.2 Improved signal sensing method based on the scale transformation of the variable step-size intermittent chaotic differential dual-coupled Duffing oscillator

Although the signal sensing method of the intermittent chaotic dual-coupled Duffing oscillator improves the speed and accuracy of a certain SNR ratio and threshold solution, it still cannot solve the problem of estimating the unknown frequency signal parameters and the high SNR ratio threshold [50]. In this paper, combining the theoretical knowledge of scale transformation and variable step-size method, an improved signal sensing method based on the scale transformation of the variable step size intermittent chaotic differential dual-coupled Duffing oscillator is proposed. The sensed unknown signal frequency's estimated result is more accurate, the SNR ratio threshold is lower, and the calculation overhead is smaller.

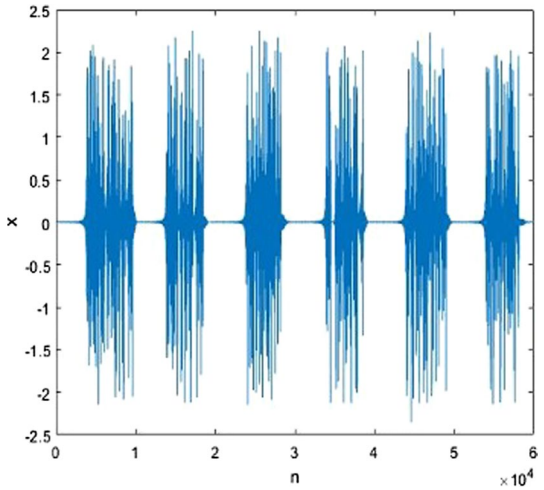

Fig. 10 Differential sequence diagram of intermittent chaotic state

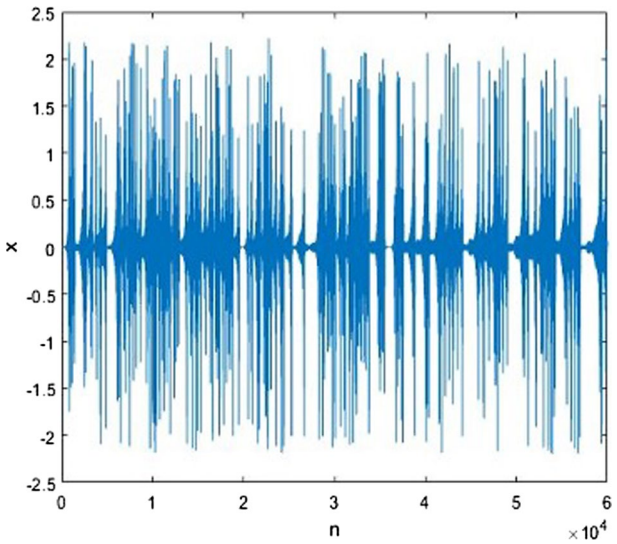

Fig. 11 Differential sequence diagram of chaotic state

$$\begin{cases} \ddot{x_1}(t) + k\dot{x_1}(t) - x_1(t) + x_1^3(t) + d\big(y_1(t) - x_1(t)\big) & = Fcos(\omega t) + Acos(\omega_1 t) \\ \ddot{y_1}(t) + k\dot{y_1}(t) - y_1(t) + y_1^3(t) + d\big(x_1(t) - y_1(t)\big) & = Fcos(\omega t) + Acos(\omega_1 t) \\ \ddot{x_2}(t) + k\dot{x_2}(t) - x_2(t) + x_2^3(t) + d\big(y_2(t) - x_2(t)\big) & = \xi \cdot Fcos(\omega t) + Acos(\omega_1 t) \\ \ddot{y_2}(t) + k\dot{y_2}(t) - y_2(t) + y_2^3(t) + d\big(x_2(t) - y_2(t)\big) & = \xi \cdot Fcos(\omega t) + Acos(\omega_1 t) \end{cases} \tag{22}$$

where ξ is the influencing parameter of the chaotic oscillator; the other parameters of the two pairs of Duffing oscillators are the same. By generating the differential timing diagrams $x_1(t) - x_2(t)$ of the two pairs of Duffing oscillators to observe whether the signal has been sensed, the timing diagram should be regular. The change of ξ will not affect the waveform, only the magnitude of the phase difference. When $\xi = 1$ the phase difference disappears, and the two pairs of oscillators are the same. At this time, they will

degenerate into ordinary dual-coupled Duffing oscillators. In this paper, through many experiments, the final choice of $\xi = 1.001$ has obtained a more intuitive effect.

In this paper, the fourth-order Runge--Kutta method is used to analyze the Duffing vibrator sensing system numerically. Through calculation, when the frequency difference range of intermittent chaos is $\left|\frac{\Delta\omega}{\omega}\right| < 0.09$, the system is in the state of intermittent chaos. Comparing the intermittent chaotic frequency difference range of the three methods, we can get that the method proposed in this paper can better sense the step size, which makes the use of the variable step-size method more meaningful and can more easily realize the signal sensing of unknown frequencies. The intermittent chaotic sequence diagram of the method proposed in this paper is shown in Fig. 12:

Next, apply variable step size on the basis of the above. Change the solution step length of the solution process, and convert the signal into the corresponding discrete sequence of the built-in driving force of the sensing system. By observing the system output $x_1(t)$ timing diagram and $x_1(t) - x_2(t)$ differential timing diagram to determine whether the sensing is successful. Let the angular frequency of the built-in signal of the sensing system be ω For the signal to be measured with an angular frequency of ω_1, the conventional system solution step is the interval of the built-in driving force sequence of the sensing system, the sequence interval of the signal to be sensed is $T_s(T_s = \frac{1}{f_s}$, f_s is the sampling rate of the signal). The sensing result is only related to the sampling rate and has nothing to do with the step length. Therefore, the built-in driving force sequence interval of the sensing system can be changed until the system is adjusted to an intermittent chaotic state, thereby completing signal sensing.

The total strategy term of equation (15) is $Fcos(\omega t) + Acos(\omega_1 t)$ and $\xi Fcos(\omega t) + Acos(\omega_1 t)$. When the system is in an intermittent chaotic state, set the built-in driving force sequence interval to $\frac{\dot{\omega}}{s\omega f_s}$, $\dot{\omega} = \omega + \Delta\omega$, $s \in (0.91, 1.09)$. This is equivalent to changing the signal to be measured by $\frac{\Delta\omega}{\omega}$ times on the time axis, so that the relative angular frequency with the built-in signal becomes $1:1$. Under this condition, the influence of the signal under test on the output phase of the system is equivalent to a signal with the same frequency as the built-in driving force. This means that the improved algorithm for the built-in signal angular frequency ω can transform the step size to make the signal under test whose frequency is not in the

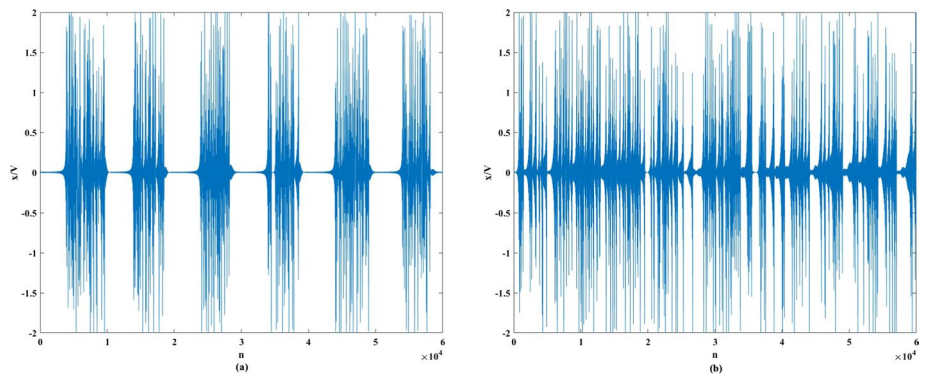

Fig. 12 The output sequence of improved method

range of $(0.91, 1.09)\omega$, and it can also make the sensing system appear intermittent chaotic. When the variable step size method is applied, the two strategy items are discretized as follows:

$$\begin{cases} L_{n_1} = Fcos\left(\frac{n\dot{\omega}}{sf_s}\right) + Acos\left(\frac{n\dot{\omega}}{f_s}\right) \\ L_{n_2} = \xi \cdot Fcos\left(\frac{n\dot{\omega}}{sf_s}\right) + Acos\left(\frac{n\dot{\omega}}{f_s}\right) \end{cases} \tag{23}$$

At this time, reconstruct a new chaotic oscillator sequence with length n and a common ratio $\left|\frac{\omega+\Delta\omega}{\omega}\right|$ satisfying $\left|\frac{\Delta\omega}{\omega}\right| < 0.09$. The sequence is expressed as:

$$\omega_1 = 1, \quad \omega_2 = \left|\frac{\omega+\Delta\omega}{\omega}\right|\omega_1, \quad \omega_3 = \left|\frac{\omega+\Delta\omega}{\omega}\right|\omega_2, \ldots, \omega_n = \left|\frac{\omega+\Delta\omega}{\omega}\right|\omega_{n-1} \tag{24}$$

Bring the oscillator array into (12) to find the critical chaotic state frequency difference threshold of the sensing system under the current chaotic oscillator array, and adjust the built-in driving force sequence interval $a_n = 2\pi\frac{s^n}{s\omega f_s}$, $(n = 1, 2, \ldots, N)$ and observe the system output timing diagram, if the frequency difference between the built-in driving force and the signal meets the standard of intermittent chaos, the sensing system will appear intermittent chaos. The specific steps are shown in Fig. 13.

When two adjacent built-in driving force sequence intervals are in an intermittent chaotic state, the existence and frequency range of the signal to be measured can be determined. When the noise intensity is too high, the state of the Duffing oscillator's sensing system will be significantly affected by the noise, which will cause the system to enter the wrong chaotic state, and make the weak signal sensing wrong, as shown in Fig. 14.

Therefore, this paper adopts the method of calculating the standard deviation σ_s of the input signal and automatically scales the signal under test superimposed with noise through the standard deviation. First, collect a piece of input signal $f(t)$ of length N, calculate the standard deviation of the sampling sequence $\sigma_s^2 = Ex^2 - E^2x$, and set a target standard deviation value σ_{sd} based on this. Then calculate the standard deviation of the collected signals once and construct the scale conversion factor $k = \frac{\sigma_{sd}}{\sigma_s}$. If

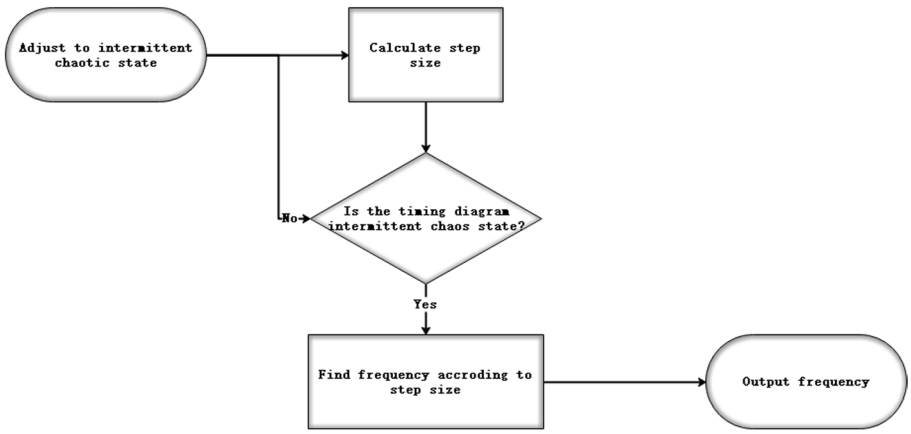

Fig. 13 The specific steps of the chaotic sensing system

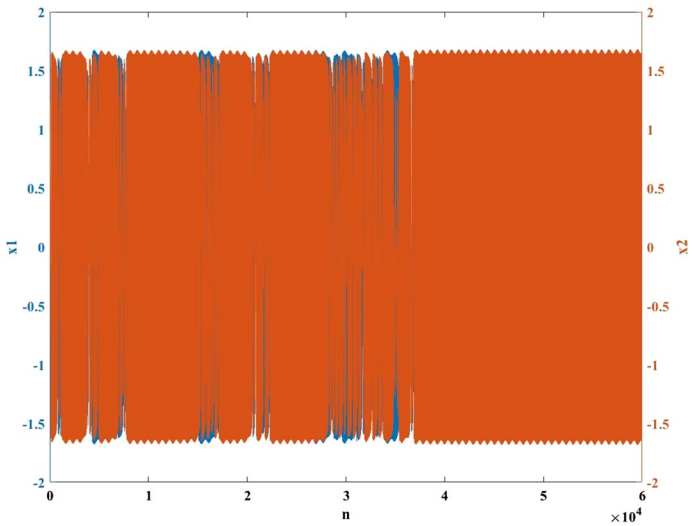

Fig. 14 The wrong chaotic state of the chaotic sensing system

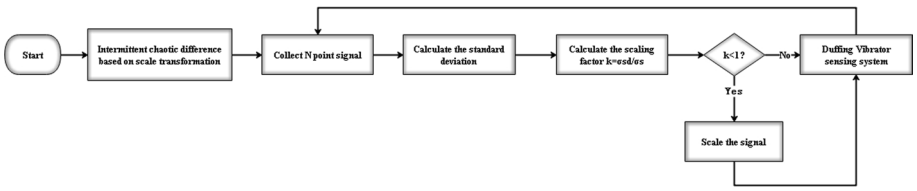

Fig. 15 The scale transformation flow chart

$k < 1$, multiply the sampled signal by k to obtain the transformed sample sequence, and then send it to the signal sensing system. Let the strategy term after the equation be $U(t) = A\frac{\sigma_{sd}}{\sigma_s}cos(\omega_1 t)$. The system expression using scale transformation is as follows:

$$\begin{cases} \ddot{x_1}(t) + k\dot{x_1}(t) - x_1(t) + x_1^3(t) + d\big(y_1(t) - x_1(t)\big) = Fcos(\omega t) + U(t) \\ \ddot{y_1}(t) + \alpha\dot{y_1}(t) + \alpha y_1^2(t)\dot{y_1}(t) + y_1(t) + d\big(x_1(t) - y_1(t)\big) = Fcos(\omega t) + U(t) \\ \ddot{x_2}(t) + k\dot{x_2}(t) - x_2(t) + x_2^3(t) + d\big(y_2(t) - x_2(t)\big) = \xi Fcos(\omega t) + U(t) \\ \ddot{y_2}(t) + \alpha\dot{y_2}(t) + \alpha y_2^2(t)\dot{y_2}(t) + y_2(t) + d\big(x_2(t) - y_2(t)\big) = \xi Fcos(\omega t) + U(t) \end{cases} \tag{25}$$

The parameters shown in Fig. 15 are added to the sensing system after the scale transformation is introduced, and the output state is shown in Fig. 16. It can be seen that the anti-interference ability of the sensing system against noise is significantly improved after the scale conversion is added. The sensing SNR ratio threshold is obviously reduced.

4 Experiment and analysis

In order to describe the actual marine environment more effectively, this paper first uses the Chambers-Mallows-Stuck (CMS) method to generate Lévy noise with $D = 1$, The values of α are 1.5, 1.8 and 2. Under the interference of the Lévy noise model, an intermittent chaotic signal sensing system based on the improved scale transform intermittent chaotic

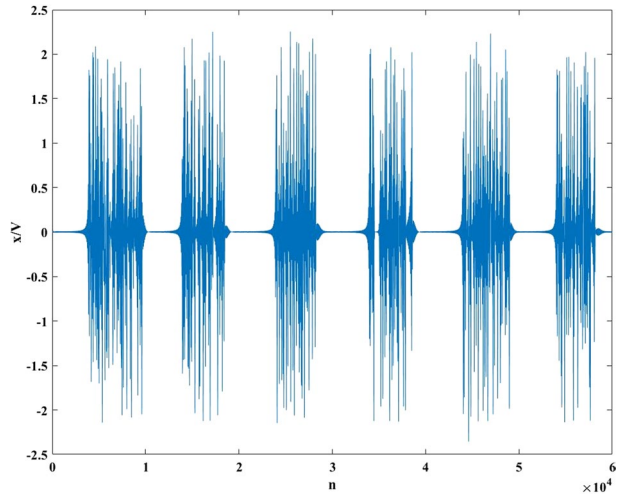

Fig. 16 Intermittent chaos sensing system with scale conversion

variable step size dual-coupled Duffing oscillator is established. The simulation proves the efficiency and superiority of the sensing system. Finally, to verify the effectiveness of the actual application of the method in this paper, the underwater acoustic data of a reservoir in Sichuan are used for the experiment.

4.1 Sensing results of each intermittent chaotic sensing system

4.1.1 Single Duffing oscillator

Firstly, the sensing performance of intermittent chaos sensing system based on single Duffing oscillator under the background of Lévy noise is studied and analyzed. Create a new chaotic oscillator column with the common ratio of $q = 1.03$, and then use the frequency scanning to sense the weak signal of unknown frequency to be measured. The range that each oscillator in the oscillator column can scan is $0.01\omega \leq |\Delta\omega| \leq 0.03\omega$. When there is intermittent chaotic state between two adjacent oscillators, the frequency range of the signal to be measured can be determined immediately. Through the experimental analysis in the previous section, it is found that when $\left|\frac{\Delta\omega}{\omega}\right| \leq 0.03$, the intermittent chaos sensing system of single Duffing oscillator can accurately show the phenomenon of intermittent chaos. Select appropriate parameters to enable the system to accurately show intermittent chaos. At this time, $\Delta\omega = \pm 0.03\omega$ is selected as the common ratio to build a group of chaotic oscillator columns with a length of:

$$\omega_1 = 1, \quad \omega_2 = \left|\frac{\omega + \Delta\omega}{\omega}\right|\omega_1, \quad \omega_3 = \left|\frac{\omega + \Delta\omega}{\omega}\right|\omega_2, \quad \ldots, \quad \omega_n = \left|\frac{\omega + \Delta\omega}{\omega}\right|\omega_{n-1} \tag{26}$$

When the frequency of the weak signal of the period to be measured is not available, in order that the chaotic system can finally reflect the frequency range of the signal to be measured, first replace each item of formula 26 with formula 25 for calculation, then find the appropriate critical chaotic threshold through experiments, calculate and obtain the value of γ, and judge it through the timing diagram output by the intermittent chaotic

sensing system of single Duffing oscillator. When intermittent chaos occurs in adjacent oscillators, the frequency of the signal to be measured can be limited.

Let the signal to be measured be $f(t) = A\cos(10t) + \eta(t)$, $\eta(t)$ represent the Lévy noise with characteristic index $\alpha = 1.5$, deflection parameter $\beta = 0$ and noise intensity $D = 0.1$. Input the signal to be measured into the intermittent chaos sensing system of single Duffing oscillator, and adopt the above sensing method. After multiple experimental sensing, when the chaotic oscillator is in $\omega_7 7$ and $\omega_7 8$, the time sequence diagram output by the system is a clear intermittent chaos state, the angular frequency ω of the signal to be measured is estimated to be $\frac{\omega_{77}+\omega_{78}}{2} = 9.883991$, and the deviation rate is about 1.1%. The sensing results are shown in Fig. 17.

When the amplitude of the signal to be measured is $A = 0.37$, the output of the single Duffing oscillator intermittent chaos sensing system is an obvious intermittent chaos phenomenon, which shows that the intermittent chaos sensing system can successfully sense the signal to be measured with unknown frequency under Lévy noise at this time. When the amplitude of the signal to be measured is $A < 0.37$, the system cannot output a relatively stable intermittent chaos phenomenon. Therefore, under this condition, the signal to be tested with unknown frequency cannot be sensed successfully. Through following formula 27, it can be calculated that the minimum signal-to-noise ratio of the signal to be measured with unknown frequency that the system can sense at this time is 7.6192 dB.

$$\mathrm{SNR} = 10\lg\left(\frac{P_{\mathrm{signal}}}{P_{\mathrm{noise}}}\right) = 10\lg\left(\frac{\lim\limits_{\Delta\omega\to 0}\int_{\omega_0-\Delta\omega}^{\omega_0+\Delta\omega} X^2(\omega)\mathrm{d}\omega}{\int_{\omega_c-}^{\omega_c+} X^2(\omega)\mathrm{d}\omega - \lim\limits_{\Delta\omega\to 0}\int_{\omega_0-\Delta\omega}^{\omega_0+\Delta\omega} X^2(\omega)\mathrm{d}\omega}\right) \quad (27)$$

where $X(\omega)$ is the Fourier transform of the system output, $\omega_{c+}$and $\omega_{c-}$are the upper boundary cutoff frequency and lower boundary cutoff frequency of intercepting the system output signal, $\omega_0 \in [\omega_{c+}, \omega_{c-}]$.

4.1.2 Dual-coupled Duffing oscillator

Secondly, the sensing performance of intermittent chaos sensing system based on dual-coupled Duffing oscillator under the background of Lévy noise is studied and analyzed. Through the experimental analysis in the previous section, it is found that when

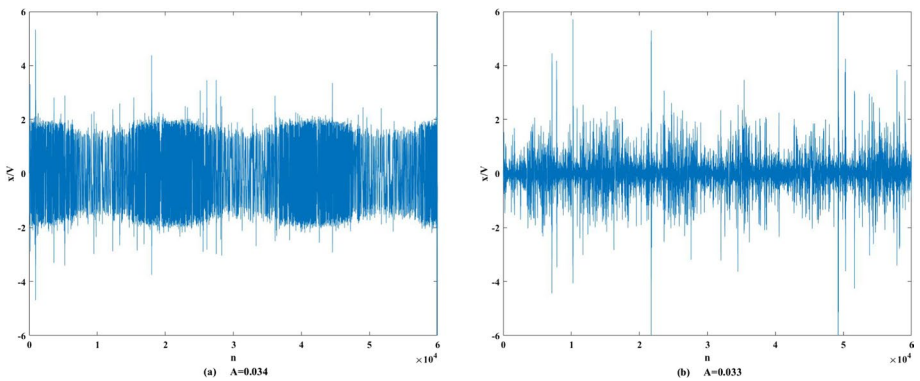

Fig. 17 The intermittent chaotic single Duffing vibrator sensing system

$\left|\frac{\Delta\omega}{\omega}\right| \leq 0.08$, the intermittent chaos sensing system of single Duffing oscillator can accurately show the phenomenon of intermittent chaos. Select appropriate parameters to enable the system to accurately show intermittent chaos. At this time, $\Delta\omega = \pm 0.08\omega$ is selected as the common ratio to build a group of chaotic oscillator columns with a length of:

$$\omega_1 = 1, \quad \omega_2 = \left|\frac{\omega + \Delta\omega}{\omega}\right|\omega_1, \quad \omega_3 = \left|\frac{\omega + \Delta\omega}{\omega}\right|\omega_2, \quad \ldots, \quad \omega_n = \left|\frac{\omega + \Delta\omega}{\omega}\right|\omega_{n-1} \tag{28}$$

When the frequency of the weak signal of the period to be measured is not available, in order that the chaotic system can finally reflect the frequency range of the signal to be measured, first replace each item of formula (28) with formula (27) for calculation, and then calculate the values of x_1 and x_2 after finding the appropriate critical chaotic threshold through experiments, and judge by coupling the $x_1, 2$ sequence diagram and $x_1 - x_2$ differential sequence diagram output by the Duffing oscillator intermittent chaotic sensing system, When intermittent chaos occurs in adjacent oscillators, the frequency of the signal to be measured can be limited. Let the signal to be measured be $f(t) = A\cos(10t) + \eta(t), \eta(t)$represent the Lévy noise with characteristic index $\alpha = 1.5$, deflection parameter $\beta = 0$ and noise intensity $D = 0.1$. Input the signal to be measured into the intermittent chaos sensing system of single Duffing oscillator, and adopt the above sensing method. After multiple experimental sensing, when the chaotic oscillator is in $\omega_2 9$ and $\omega_3 0$, the time sequence diagram output by the system is a clear intermittent chaos state, the angular frequency ω of the signal to be measured is estimated to be $\frac{\omega_{29}+\omega_{30}}{2} = 9.6896$, and the deviation rate is about 3.1%. The sensing results are shown in Fig. 18.

When the amplitude of the signal to be measured is $A = 0.096$, the output of the single Duffing oscillator intermittent chaos sensing system is an apparent intermittent chaos phenomenon, which shows that the intermittent chaos sensing system can successfully sense the signal to be measured with an unknown frequency under Lévy noise at this time. When the signal amplitude to be measured is $A < 0.096$, the system cannot output a relatively stable intermittent chaos phenomenon. Therefore, the signal tested with an unknown frequency cannot be sensed successfully under

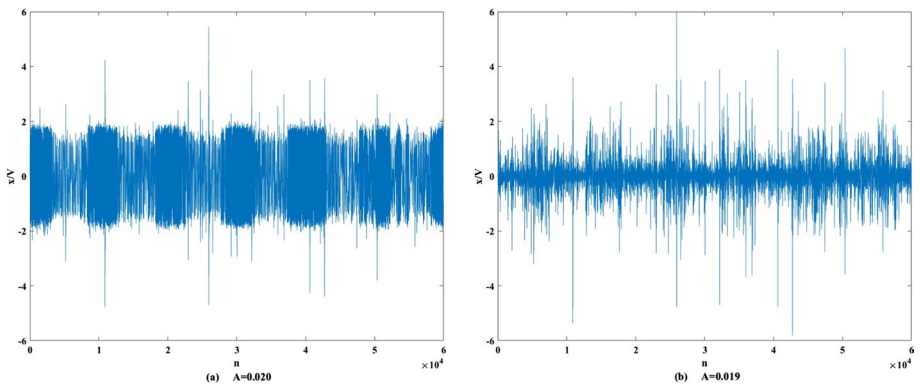

Fig. 18 The intermittent chaotic dual-coupled Duffing oscillator sensing system

this condition. Through following formula 27, it can be calculated that the minimum signal-to-noise ratio of the signal to be measured with an unknown frequency that the system can sense at this time is − 3.3649 dB.

4.1.3 Our sensing system

Next, the sensing performance of intermittent chaos sensing system based on dual-coupled Duffing oscillator under the background of Lévy noise is studied and analyzed. Let the signal to be measured be $f(t) = A\cos(10t) + \eta(t)$, $\eta(t)$represent the Lévy noise with characteristic index $\alpha = 1.5$, deflection parameter $\beta = 0$ and noise intensity $D = 0.1$. After generating the above-mentioned Lévy noise model, take $a_n = 2\pi\frac{s^n}{s\omega f_s}$ as the solution step size of the sensing system, and $A\frac{\sigma_{sd}}{\sigma_s}cos(\omega_1 t) + \eta(t)$ as the input signal, $\eta(t)$ is the generated Lévy noise. The specific steps of the intermittent chaotic signal sensing system based on the scale transformation variable step size dual-coupled Duffing oscillator established in this paper are as follows:

1. Use the scale transformation method to pretreat the signal.
2. Adjust the parameters of the intermittent chaotic signal sensing system of the variable-step dual-coupled Duffing oscillator, and set $F = 0.789$, $\omega_1 = 1rad/s$, $\alpha = 1.001$, $d = 0.2$.
3. The processed signal $Acos\left(\omega_1\frac{\sigma_{sd}}{\sigma_s}t\right) + \eta(t)$ s input into the sensing system as the input signal, the frequency is set to 1 kHz, and the initial solution step is set to $a_n = 2\pi\frac{s^n}{s\omega f_s}, n = 1, 2, \ldots, N$.
4. Adjust the solution step length and observe the $x_1(t) - x_2(t)$ timing diagram output. If the sensing system has an intermittent chaotic state between two adjacent steps a_n and a_{n+1}, then it indicates that the signal has been sensed, otherwise return 2.
5. If the signal has been sensed, the angular frequencies ω_n and ω_{n+1} corresponding to solution step size are a_n and a_{n+1} can be calculated by $\omega_n = s^n rad/s$, then the angular frequency of the sensed signal $\ddot{\omega} = \frac{\omega_n+\omega_{n+1}}{2}rad/s$. Using the above sensing method, after many experimental tests, when the step size is $a_3 9$ and $a_4 0$, the timing diagram output by the system is in a clear intermittent chaotic state, the angular frequency ω of the signal to be measured is estimated to be $\frac{\omega_{39}+\omega_{40}}{2} = 9.9946$,, and the deviation rate is 0.054%. The sensing results are shown in Fig. 19.

When the amplitude of the signal to be measured is $A = 0.010$, the output of the single Duffing oscillator intermittent chaos sensing system is an apparent intermittent chaos phenomenon, which shows that the intermittent chaos sensing system can successfully sense the signal to be measured with an unknown frequency under Lévy noise at this time. When the signal amplitude to be measured is $A < 0.010$, the system cannot output a relatively stable intermittent chaos phenomenon. Therefore, the signal tested with an unknown frequency cannot be sensed successfully under this condition. Through following formula 27, it can be calculated that the minimum signal-to-noise ratio of the signal to be measured with an unknown frequency that the system can sense at this time is − 23.9254 dB.

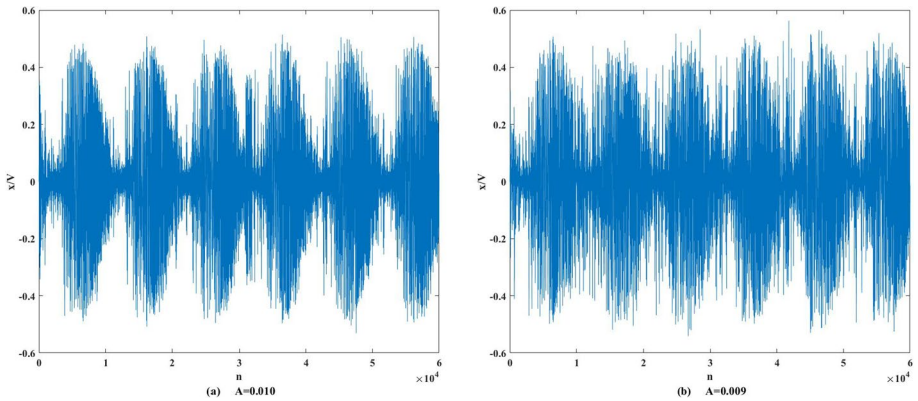

Fig. 19 The intermittent chaotic single Duffing vibrator sensing system

4.2 Sensing performance analysis of our system

4.2.1 Influence of coupling coefficient on our sensing system

Under normal circumstances, the higher the coupling strength of the system, the stronger the synchronization between the oscillators. D in formula (18) represents the coupling coefficient. In order to further compare the noise immunity and stability of the coupling system corresponding to different coupling coefficients, the concept of standard deviation is introduced:

$$\sigma = \sqrt{\frac{1}{N-1}\sum_{t=1}^{N}[x_n(t) - x_0(t)]^2} \tag{29}$$

Calculate the standard deviation of different coupling coefficients d under different noise backgrounds, as shown in Tables 1 and 2:

It can be seen from Tables 1 and 2 that as the intensity of noise changes, the standard deviation of the sensing system gradually changes for any system, the smaller the standard deviation, the stronger the stability of the system. According to the research in the above table, this paper chooses the coupling coefficient $d = 0.2$ in order to obtain the optimal performance of the system.

4.2.2 Influence of Lévy noise impact on our sensing system

The signal to be measured $f(t) = Acos(10t)$ is superimposed with different Lévy noise $\eta(t)$ and then input into three systems for sensing. From Fig. 15a, it can be seen that the single Duffing vibrator and the dual-coupled Duffing vibrator have weaker sensing of weak signals under the background of strong impact Lévy noise ($\alpha = 1.5, 1.8$) and have the weak noise immunity. The sensing system established in this paper can clearly sense the weak signal under the strong impact of Lévy noise ($\alpha = 1.5, 1.8$) and has strong anti-interference (Fig. 20).

Table 1 The standard deviation of different coupling coefficients d under different noise backgrounds ($D = 1$)

d/α	$\alpha = 1.5$	$\alpha = 1.8$	$\alpha = 2$
$d = 0$	1.906	1.057	1.054
$d = 0.1$	1.095	1.039	1.034
$d = 0.2$	1.039	0.972	0.96
$d = 0.3$	1.056	0.988	0.977
$d = 0.4$	1.068	1.004	0.996
$d = 0.5$	1.082	1.022	1.015

Table 2 The standard deviation of different coupling coefficients d under different noise backgrounds ($D = 0.5$)

d/α	$\alpha = 1.5$	$\alpha = 1.8$	$\alpha = 2$
$d = 0$	1.058	1.054	1.052
$d = 0.1$	1.053	1.034	1.032
$d = 0.2$	0.987	0.955	0.947
$d = 0.3$	1.003	0.974	0.968
$d = 0.4$	1.019	0.994	0.99
$d = 0.5$	1.035	1.014	1.011

4.2.3 Multi-frequency signal sensing performance

In actual underwater signal sensing, multiple signals will be sensed. We change the input signal to $0.01cos(10t) + 0.01cos(20t)$, and the Lévy noise takes $\alpha = 1.5$, respectively, $(\eta(t))$. The sensing results are shown in Figs. 21 and 22.

From Figs. 21 and 22, the sensing system established in this paper can show intermittent chaos when sensing two signals of different frequencies. The signals of the two frequencies are sensitive, so it cannot be determined that the signal can be sensed. Therefore, the method proposed in this paper has obvious advantages in sensing unknown signals in multiple frequency bands.

When the solution step size is a_{39} and a_{40}, the corresponding sizes of f_{39} and f_{40} are 9.87 Hz and 10.08 Hz, respectively, and then the judgment frequency of the sensing system established in this paper is $f_{10} = 10$ Hz. When the solution step size is a_{51} and a_{52}, the corresponding sizes of f_{51} and f_{52} are 19.77 Hz and 20.10 Hz, respectively, and the sensing system judges the frequency of the signal is $f_{20} = 20$ Hz. When frequencies are 10 Hz and 20 Hz, the calculation error rate is less than 0.03%, that is, it can obtain the frequency of the signal to be sensed more accurately under the interference of a strong noise environment.

4.2.4 Actual underwater acoustic data sensing

Figure 23 shows the low-frequency underwater data collected by a reservoir in Sichuan Province, China. In order to facilitate the analysis, the actual underwater acoustic data were sampled again at a sampling frequency of 1 kHz. After obtaining the underwater acoustic signal data, the normalization operation was carried out and

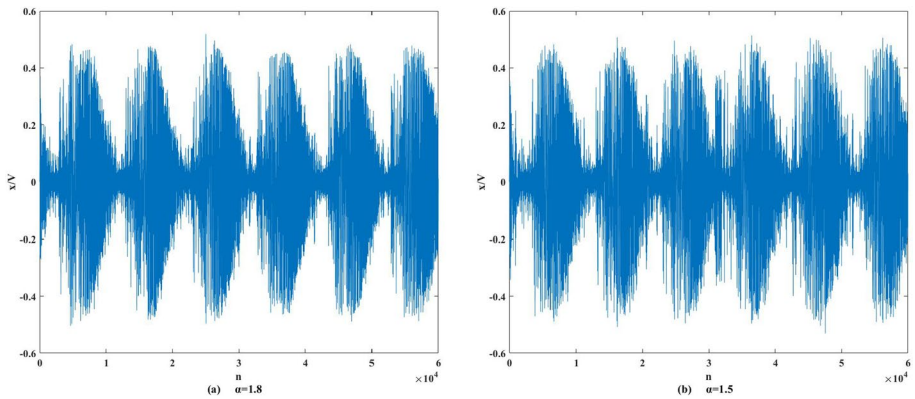

Fig. 20 Our sensing system

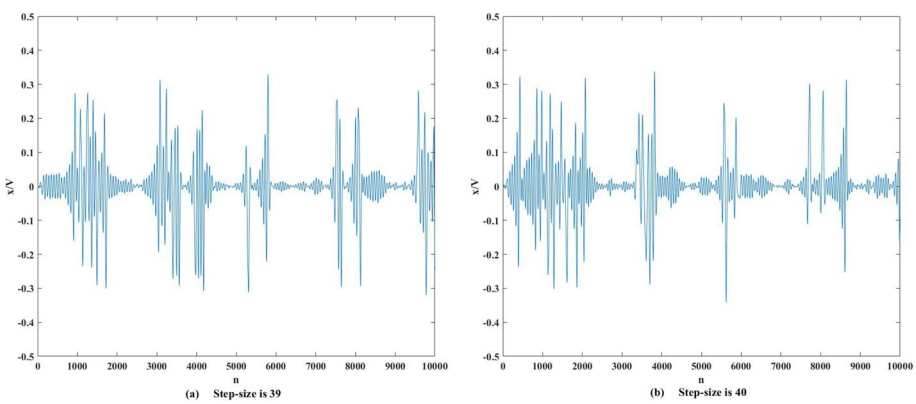

Fig. 21 The sensing result of the first segment of the multi-frequency signal

then sent to the sensing system based on this paper. From Fig. 23, it can be found that there is strong impulsive noise underwater and strong broadband interference noise at many moments, which is more consistent with the Lévy noise generated by simulation, which shows that it is reasonable and appropriate to use Lévy noise to describe underwater environmental noise.

Figure 24 is the power spectral density diagram of the signal. It can be observed that the approximate signal frequency is about 10 Hz. In order to sense the actual signal, we set the initial solution step size is $a_n = 2\pi \frac{s^n}{s\omega f_s}$, $s = 1.06$ and input the actual signal into the sensing system established in this paper to obtain the result as shown in Fig. 25:

In Fig. 25, the step size of the sensing system is a_{39} and a_{40}, it shows an obvious intermittent chaotic state. The corresponding magnitudes of f_{39} and f_{40} are 9.87 Hz and 10.08 Hz, respectively, and the system judges that the frequency of the signal which to be sensed at this time is $f_{10} = 9.99$ Hz. When the frequency of the signal to be measured is 10 Hz, the calculation error rate is less than 0.02%. Our sensing system is more accurately under the interference of a strong natural environment. It verifies

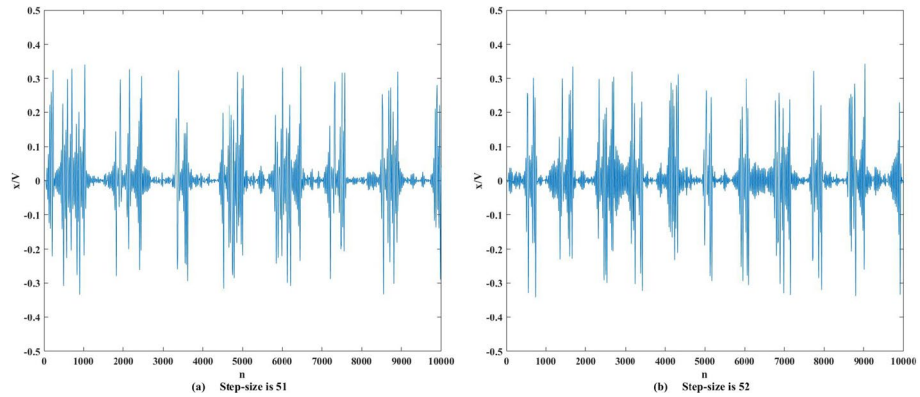

Fig. 22 The sensing result of the second segment of the multi-frequency signal

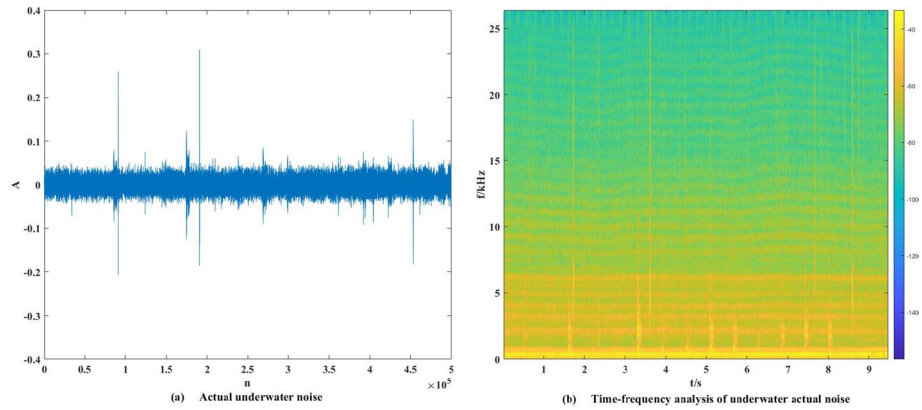

Fig. 23 Actual underwater acoustic data

the effectiveness and scientificity of the sensing system established in this paper in practical applications.

5 Results and discussion

The signal sensing results of each chaotic system established under the background of Lévy noise are summarized in Table 3.

The signal frequency estimation results of each chaotic system established under the background of Lévy noise are summarized in Table 4.

Since the sensing method proposed in this paper can change the common ratio to form a new solution step size and sensing bandwidth, the number of solution steps is reduced, thereby reducing the amount of calculation better. The data of each sensing system are shown in Table 5.

It can be seen from Table 5 that the number of solving steps and the amount of calculation of the sensing system established in this paper are obviously the smallest. Through Tables 3, 4 and 5, it is found that under the Lévy noise with characteristic index $\alpha = 1.5$, deflection parameter $\beta = 0$ and noise intensity $D = 0$, the sensing

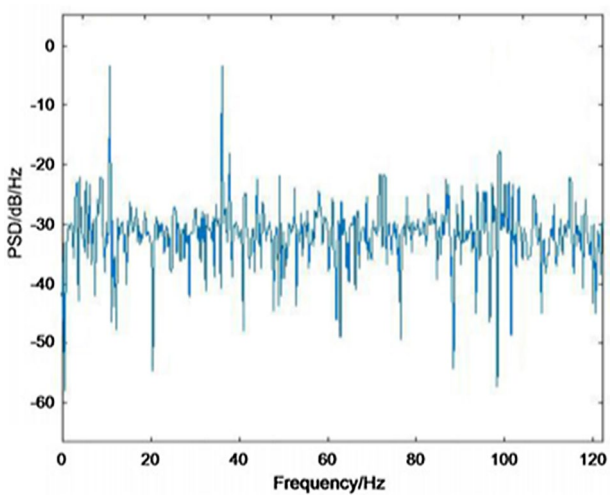

Fig. 24 Power spectral density diagram

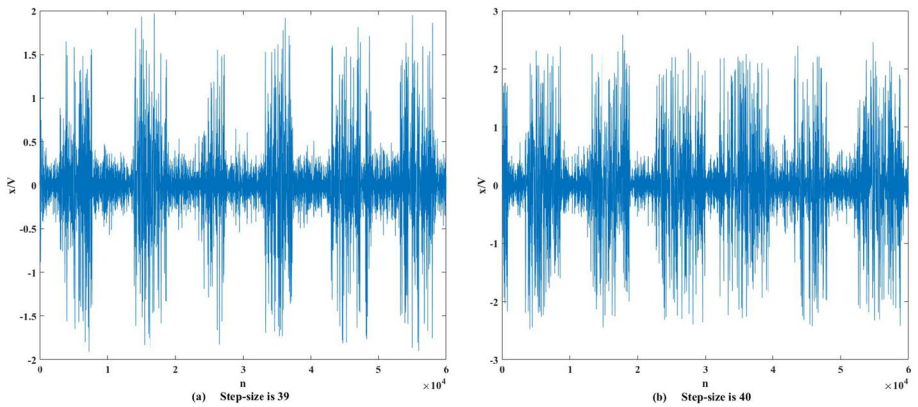

Fig. 25 The sensing result of the actual underwater acoustic data

Table 3 Signal sensing results of intermittent chaotic systems under the Lévy noise with characteristic index $\alpha = 1.5$, deflection parameter $\beta = 0$ and noise intensity $D = 0.1$

Method	Minimum signal amplitude (V)	Minimum SNR ratio (dB)
Single Duffing oscillator	$A = 0.340$	7.61920
Double Duffing oscillator	$A = 0.096$	− 3.3649
Ours	$A = 0.010$	− 23.9254

deviation rate of single Duffing oscillator intermittent chaotic sensing system for weak signals with unknown frequency is 1.1%, the minimum signal amplitude that can be sensed is $A = 0.34$, and the lowest sensing signal-to-noise ratio is 7.61920; the sensing deviation rate of the coupled Duffing oscillator intermittent chaotic sensing system

Table 4 Signal frequency estimation results of intermittent chaotic systems under the Lévy noise with characteristic index $\alpha = 1.5$, deflection parameter $\beta = 0$ and noise intensity $D = 0.1$

Method	Actual frequency (Hz)	Estimation frequency	Estimation error rate
Single Duffing	10	9.8840	3.1%
Double Duffing	10	9.6896	1.1%
Ours	10	9.9946	0.054%

Table 5 Data of each sensing system

Method	Common ratio	Number of solving steps	Sensing bandwidth
Single Duffing oscillator	1.01	282	$(1.00, 1.01)\omega$
	1.02	197	$(0.99, 1.02)\omega$
	1.03	98	$(0.98, 1.03)\omega$
Double Duffing oscillator	1.05	68	$(0.97, 1.05)\omega$
	1.06	60	$(0.96, 1.06)\omega$
	1.07	57	$(0.95, 1.07)\omega$
Ours	1.06	60	$(0.96, 1.06)\omega$
	1.07	57	$(0.95, 1.07)\omega$
	1.08	35	$(0.94, 1.08)\omega$

for weak signals with unknown frequency is 3.1%, the minimum signal amplitude that can be sensed is 0.096, and the minimum sensing signal-to-noise ratio is − 3.3646 dB; the sensing deviation rate of our sensing system for weak signals with unknown frequency is 0.054%, the lowest signal amplitude that can be sensed is $A = 0.010$, and the lowest sensing signal-to-noise ratio is − 23.9254 dB. Finally, through the experiments in the previous section, it is found that the sensing scheme proposed in this paper has a certain immunity to the impact of Lévy noise and noise of different intensities; it can successfully and accurately obtain the frequency of multi-frequency weak signal to be measured, and the estimation error is 0.33%, which has strong system stability.

6 Conclusions

This paper has proposed a Lévy noise model to describe the underwater natural environment under substantial interference for the underwater information sensing task. It describes the actual underwater environment more accurately and provides an analysis and estimation method to select better parameters; aiming at the sensing problem of the unknown frequency signal under the Lévy noise, this paper has proposed an improved dual-coupled Duffing oscillator signal sensing method based on the variable step-size method and scale transformation. The method has better resistance to intense noise, better adaptability to all kinds of impact noise, higher sensing efficiency, more intuitive sensing results, and lower SNR ratio threshold; under the interference of Lévy noise, the improved dual-coupled Duffing oscillator signal sensing system based on variable step size intermittent chaos has established. A large number of simulation experiments show the effectiveness and superiority of the system. The lowest SNR threshold is − 23.9254

dB. The error rate of frequency estimation is 0.33%. Finally, experiments are carried out with actual underwater acoustic data to verify the effectiveness and scientificity of the sensor system established in this paper in practical application.

Acknowledgements
We gratefully acknowledge the people who gave meticulous and valuable comments on this paper and the anonymous reviewers who spent the valuable time in reviewing our paper.

Author contributions
All authors reviewed and edited the manuscript. All authors read and approved the final manuscript.

Funding
This work was supported in part by the National Natural Science Foundation of China (Nos. 62072074, 62076054, 62027827, Nos. 61902054, 62002047), the Frontier Science and Technology Innovation Projects of National Key R&D Program (No. 2019QY1405), the Sichuan Science and Technology Innovation Platform and Talent Plan (No. 2020JDJQ0020), the Sichuan Science and Technology Support Plan (No. 2020YFSY0010).

Availability of data and materials
The datasets generated or analyzed during the current study are not publicly available due [REASON WHY DATA ARE NOT PUBLIC] but are available from the corresponding author on reasonable request.

Declarations

Consent for publication
All authors have agreed and given their consent for submission of this paper to Euraship Journal of Wireless Communication.

Competing interests
The authors declare that they have no competing interests.

Author details
[1]School of Automation Engineering, University of Electronic Science and Technology of China, Chengdu, China. [2]School of Physical Science and Technology, Southwest Jiaotong University, Chengdu, China. [3]Network and Data Security Key Laboratory of Sichuan Province, Chengdu, China.

Received: 7 January 2022 Accepted: 29 March 2022
Published online: 03 May 2022

References

1. D. Chen, Z. Zhao, X. Qin, Y. Luo, M. Cao, H. Xu, A. Liu, Magleak: a learning-based side-channel attack for password recognition with multiple sensors in IIoT environment. IEEE Trans. Ind. Inf. (2020)
2. N. Zhang, P. Yang, S. Zhang, D. Chen, W. Zhuang, B. Liang, X.S. Shen, Software defined networking enabled wireless network virtualization: challenges and solutions. IEEE Netw. **31**(5), 42–49 (2017). https://doi.org/10.1109/MNET.2017.1600248
3. N. Zhang, P. Yang, J. Ren, D. Chen, L. Yu, X. Shen, Synergy of big data and 5g wireless networks: opportunities, approaches, and challenges. IEEE Wirel. Commun. **25**(1), 12–18 (2018). https://doi.org/10.1109/MWC.2018.1700193
4. H. Gao, C. Liu, A hybrid approach to trust node assessment and management for vanets cooperative data communication: historical interaction perspective. IEEE Intell. Transp. Syst. Trans. 1–10 (2021)
5. L. Ale, N. Zhang, H. Wu, D. Chen, T. Han, Online proactive caching in mobile edge computing using bidirectional deep recurrent neural network. IEEE Internet Things J. **6**(3), 5520–5530 (2019)
6. Y. Ding, G. Wu, D. Chen, N. Zhang, L. Gong, M. Cao, Z. Qin, DeepEDN: a deep-learning-based image encryption and decryption network for internet of medical things. IEEE Internet Things J. **8**(3), 1504–1518 (2020)
7. Y. Yin, Q. Huang, H. Gao, Y. Xu, Personalized APIs recommendation with cognitive knowledge mining for industrial systems. IEEE Trans. Ind. Inf. **17**(9), 6153–6161 (2021)
8. Y. Xu, Y. Wu, H. Gao, S. Song, Y. Yin, X. Xiao, Collaborative APIs recommendation for artificial intelligence of things with information fusion. Future Gener. Comput. Syst. **125**, 471–479 (2021)
9. Y. Huang, H. Xu, H. Gao, X. Ma, W. Hussain, SSUR: an approach to optimizing virtual machine allocation strategy based on user requirements for cloud data center. IEEE Trans. Green Commun. Netw. **5**(2), 670–681 (2021)
10. X. Ma, H. Xu, H. Gao, M. Bian, Real-time multiple-workflow scheduling in cloud environments. IEEE Trans. Netw. Serv. Manag. (TNSM) **18**(4), 4002–4018 (2021)
11. H. Peyvandi, M. Farrokhrooz, H. Roufarshbaf, S.-J. Park, Sonar systems and underwater signal processing: classic and modern approaches. SONAR Syst. 173–206 (2011)
12. S. Ma, H. Wang, X. Shen, H. Dong, Stochastic resonance for underwater vlf weak signal detection under lévy noise background. In: 2017 IEEE International Conference on Signal Processing, Communications and Computing (ICSPCC), pp. 1–5 (2017). IEEE
13. T. Tian, G. Liu, D. Sun, *Sonar Technology* (Harbin Engineering University Press, Harbin, 2006)
14. X. Liu, Y. Qin, Modem marine power vs state marine strategy. J. Soc. Sci. 73–79 (2004)

15. Y.L. He, Y. Wang, N. Zou, Parametric GLRT for multichannel adaptive signal detection in space-time correlated compound-gaussian disturbance. IET Radar Sonar Navig. **13**(9), 1597–1608 (2019)
16. M. Chitre, Underwater acoustic communications in warm shallow waters channels. Ph.D. thesis, National University of Singapore (2006)
17. S.B. Babarsad, S.M. Saberali, M. Majidi, Analytic performance investigation of signal level estimator based on empirical characteristic function in impulsive noise. Digit. Signal Process **92**, 20–25 (2019)
18. J.J. Jeong, S. Kim, Robust adaptive filter algorithms against impulsive noise. Circuits. Syst. Signal Process **38**(12), 5651–5664 (2019)
19. M. Hajiabadi, H. Radmanesh, M. Samkan, Robust adaptive beamforming in impulsive noise environments. IET Radar Sonar Navig. **13**(12), 2145–2150 (2019)
20. A. Korakas, J.M. Hovem, Comparison of modeling approaches to low-frequency noise propagation in the ocean. In: 2013 MTS/IEEE OCEANS-Bergen, pp. 1–7 (2013). IEEE
21. J.H. Haxel, R.P. Dziak, H. Matsumoto, Observations of shallow water marine ambient sound: the low frequency underwater soundscape of the central oregon coast. J. Acoust. Soc. Am. **133**(5), 2586–2596 (2013)
22. M. Siderius, J. Gebbie, Environmental information content of ocean ambient noise. J. Acoust. Soc. Am. **146**(3), 1824–1833 (2019)
23. R.K. Andrew, B.M. Howe, J.A. Mercer, M.A. Dzieciuch, Ocean ambient sound: comparing the 1960s with the 1990s for a receiver off the California coast. Acoust. Res. Lett. Online **3**(2), 65–70 (2002)
24. S.A. Albeverio, Y.G. Kondratiev, L. Streit, How to generalize white noise analysis to non-Gaussian measures. Dyn. Complex Irregular Syst., 120–130 (1993)
25. Y. Kondratiev, J.L. Silva, L. Streit, Generalized appell systems. Methods Funct. Anal. Topol. **3**(3), 28–61 (1997)
26. Y.G. Kondratiev, J.L. da Silva, L. Streit, Analysis on Poisson and gamma spaces. Infinice Dimens. Anal. Quantum Probab. Relat. Top. **1**(1), 91–117 (1998)
27. T. Hida, White noise analysis and its applications. In: Proceedings of the International Mathematical Conference, pp. 43–48 (1982)
28. J. Jiang, K. Wang, C. Zhang, M. Chen, H. Zheng, R. Albarracin, Sparse method for directional estimation using denoised four-order cumulants vector. Sensors **18**(6), 1815 (2018)
29. M. Yanga, Fractional stochastic differential equations driven by levy noise. Filomat **35**(7), 2403–2424 (2021)
30. S. Beltaief, O. Chernoyarov, S. Pergamenchtchikov, Model selection for the robust efficient signal processing observed with small levy noise. Ann. Inst. Stat. Math. **72**(5), 1205–1235 (2020)
31. J. Wang, J. Li, S. Yan, W. Shi, X. Yang, Y. Guo, T.A. Gulliver, A novel underwater acoustic signal denoising algorithm for gaussian/non-gaussian impulsive noise. IEEE Trans. Veh. Technol. **70**(1), 429–445 (2020)
32. S.Y. Fu, *Engineering Analysis and Application of Wavelet Transform* (Science Press, Beijing, 1999)
33. Z. Qiao, Y.L., N. Li, Applications of stochastic resonance to machinery fault detection: a review and tutorial. Mech. Syst. Signal Process. **122,** 502–536 (2019)
34. S.Q. Li, X.Z. Wu, Application of ale based on FTF algorithm in ship-radiated noise detection. Commun. Technol. **50**(6), 1175–1180 (2017)
35. S.U. Qing-wen, Z. Jin-feng, Weak signal detection based on coupled chaotic oscillator. Shijiazhuang Tiedao Univ. **32**(1), 18–23 (2019)
36. W.Y.F.H. Shao-Ping, J. Guo-Bin, Study on partial discharge signal detection by coupled duffing oscillators. Acta Phys. Sin. **62**(13) (2013)
37. N. Li, X. Li, C. Liu, Detection method of a short-time duffing oscillator array with variable amplitude coefficients. J. Harbin Eng. Univ. **37**(12), 1645–1652 (2016)
38. S. Zhou, C. Lin, Application of chaos theory for weak signal of ship detecting. J. Wuhan Univ. Technol. **33**(1), 161–164 (2009)
39. S. Li, X. Wu, Application of ale based on FTF algorithm in ship-radiated noise detection. Commun. Technol. **50**(06), 1175–1180 (2017)
40. Q. Sun, J. Zhang, Weak signal detection based on improved chaotic oscillator system with dual coupling. Comput. Mod. **1**, 17–21 (2012)
41. G. Li, Y. Hou, H. Yang, A new duffing detection method for underwater weak target signal. Alex. Eng. J.(2021)
42. S. Jing, J. Hall, Y.R. Zheng, C. Xiao, Signal detection for underwater IoT devices with long and sparse channels. IEEE Internet Things J. **7**(8), 6664–6675 (2020)
43. G.M. Moatimid, Stability analysis of a parametric duffing oscillator. J. Eng. Mech. **146**(5), 05020001 (2020)
44. M. Liu, J. Chen, H. Jiang, Z. Yu, C. Hu, B. Lu, Synchronization of chaotic delayed systems via intermittent control and its adaptive strategy. Nonlinear Anal. Model. Control **26**(6), 993–1011 (2021)
45. Z. Brzeźniak, W. Liu, J. Zhu, The stochastic strichartz estimates and stochastic nonlinear Schrödinger equations driven by levy noise. J. Funct. Anal. **281**(4) (2021)
46. W. Xu, M. Hao, X. Gu, G. Yang, Stochastic resonance induced by levy noise in a tumor growth model with periodic treatment. Mod. Phys. Lett. B **28**(11), 1450085 (2014)
47. L. Deng, X. Zhao, B. Yin, A method of extracting underwater acoustic beaconing signal. In: 2021 OES China Ocean Acoustics (COA), pp. 744–747 (2021). IEEE
48. G. Li, K. Zhao, H. Yang, A new method for detecting line spectrum of ship-radiated noise based on a new double duffing oscillator differential system (2020)
49. X. Ma, C.L. Nikias, Parameter estimation and blind channel identification in impulsive signal environments. IEEE Trans. Signal Process. **43**(12), 2884–2897 (1995)
50. X. Gu, J. Lou, K. Liu, P. Hu, Underwater detection signal based on LM-BP neural network algorithm. J. Phys. Conf. Ser. **1533** (2020)

Publisher's Note